Microsc. Microanal. 18, 1270–1284, 2012
doi:10.1017/S1431927612001122

Microscopy AND Microanalysis

REVIEW ARTICLE

Application of Cathodoluminescence Microscopy and Spectroscopy in Geosciences

Jens Götze*

Institute of Mineralogy, TU Bergakademie Freiberg, Brennhausgasse 14, D-09596 Freiberg, Saxony, Germany

Abstract: Cathodoluminescence (CL) microscopy and spectroscopy are luminescence techniques with widespread applications in geosciences. Many rock-forming and accessory minerals show CL characteristics, which can be successfully used in geoscientific research. One of the most spectacular applications is the visualization of growth textures and other internal structures that are not discernable with other analytical techniques. In addition, information from CL imaging and spectroscopy can be used for the reconstruction of processes of mineral formation and alteration to provide information about the real structure of minerals and materials, and to prove the presence and type of lattice incorporation of several trace elements. In the present article, an overview about CL properties of selected minerals is given, and several examples of applications discussed. The presented data illustrate that best results are achieved when luminescence studies are performed under standardized conditions and combined with other analytical techniques with high sensitivity and high spatial resolution.

Key words: cathodoluminescence, microscopy, spectroscopy, geosciences, quartz, feldspar, sheet silicates, apatite, zircon

Introduction

Cathodoluminescence (CL) has developed to a powerful analytical tool in many scientific fields. Minerals belong to the materials with a very long history in CL studies. Already in 1879, Crooks investigated gemstones and other minerals such as zircon during his studies with a cathode beam. Almost 100 years later, the first applications of CL with petrographic microscopes started (Sippel, 1965), and due to the development of electron beam analytics [scanning electron microscope (SEM), microprobe] first applications in this field were published in the same year (Smith & Stenstrom, 1965).

In comparison with the high-purity materials that are commonly studied by physicists and chemists, minerals and rocks are "dirty" with a lot of impurities and defects. As a result CL of minerals exhibits a number of overlapping luminescence signals that are often not easily resolved. Therefore, the application of CL studies in geosciences has developed some specific characteristics. The successful applications of CL are given in several textbooks dealing with the application of luminescence techniques in geosciences starting with the fundamental works of Marfunin in the 1970s (Marfunin, 1979). Several further publications emphasized the role of CL as a powerful technique applied to minerals and rocks (e.g., Marshall, 1988; Barker & Kopp, 1991; Götze, 2000; Pagel et al., 2000; Gorobets & Rogozine, 2002; Nasdala et al., 2004; Gaft et al., 2005; Boggs & Krinsley, 2006; Gucsik, 2009).

Received February 27, 2012; accepted April 19, 2012
*E-mail: goetze@mineral.tu-freiberg.de

Basics of Luminescence and Instrumentation

In general, luminescence is the transformation of diverse kinds of energy into visible light. It results from an emission transition of anions, molecules, or a crystal from excited electronic states to the ground state or a state with lower energy (Marfunin, 1979). The whole process includes three fundamental stages: (1) absorption of excitation energy and stimulation of the system into an excited state, (2) transformation and transfer of the excitation energy, and (3) emission of light and relaxation of the system into an unexcited condition. Details of the physical processes are often described either by using the band model or configuration coordinate diagrams (e.g., Marfunin, 1979).

Examples of luminescence processes include photoluminescence or the excitation by light [e.g., ultraviolet (UV) excitation for minerals]. Cathodoluminescence is caused by the interaction of an electron beam with a solid, which also generates backscattered and secondary electrons and characteristic X-rays.

Because luminescence of solids is dominated by defect luminescence, CL enables visualization of the real (defect) structure of minerals and materials. The defects causing CL can be related to either lattice defects (vacancies, broken bonds, etc.) or to the structural incorporation of certain trace elements (e.g., Mn^{2+}, $REE^{2+/3+}$, Cr^{3+}). Therefore, different phases can be contrasted as well as defects, zoning, and/or internal structures can be revealed using CL microscopy (CL imaging). In addition, the application of spectral CL measurements enables these defects to be determined

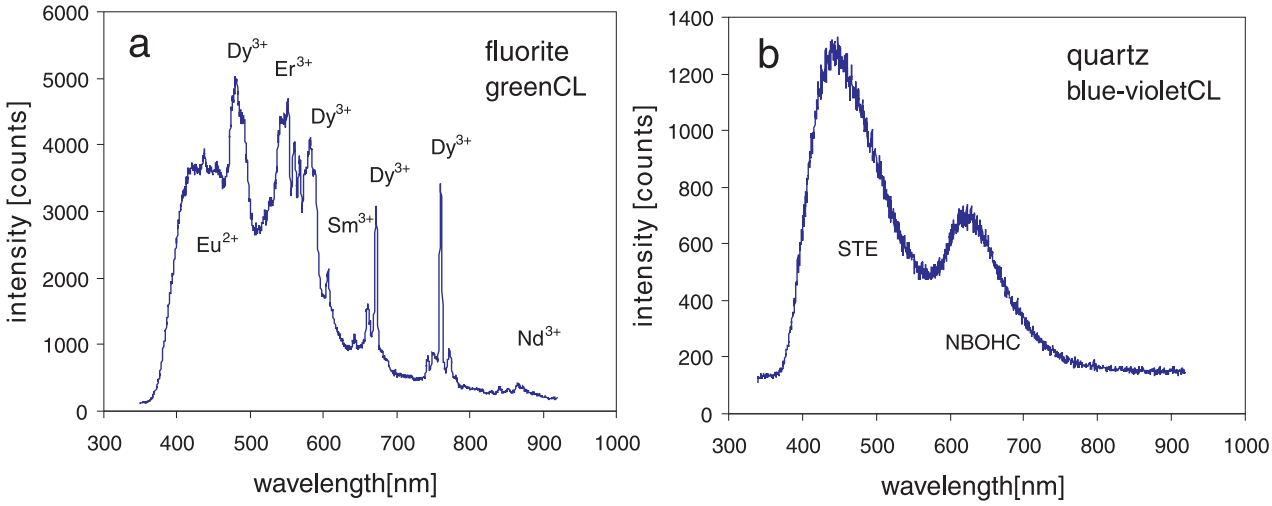

Figure 1. Two different types of CL spectra illustrate the influence of the crystal field: (**a**) sharp emission lines of REE^{3+} in green luminescent fluorite; (**b**) broad CL emission bands due to activation by lattice defects [self-trapped exciton (STE), nonbridging oxygen hole center (NBOHC)] causing bluish-violet CL in quartz.

and activator trace elements, their valence, and structural position to be detected.

For the interpretation of luminescence spectra, the interactions of luminescence centers with other constituents in the surrounding crystal lattice have to be taken into consideration (Burns, 1993). Accordingly, the luminescence of a given ion may strongly depend upon its position in the crystal and on the crystal field. If the influence of the crystal field is weak, the resulting luminescence emission is characterized by narrow emission lines without a significant Stokes shift. This is the case for most of the trivalent ions of the rare earth elements (REEs), where the electron transitions within the 4f orbitals are shielded from the influence of the crystal field by the electron shells of the 5s and 6p orbitals. Accordingly, the emission spectra are specific for each REE^{3+} ion, relatively independent on the crystal structure of the host crystal (Fig. 1a). In contrast, if the electron transitions take place in energy levels that are influenced by the local crystal field, luminescence emission spectra show relatively broad bands (Fig. 1b). Because of the dependence of the Stokes shift on the strength of the local crystal field, the wavelength of the luminescence emission of each activator element varies from mineral to mineral and is specific for the crystal structure of the host crystal. Shifts of the luminescence emission bands can also be observed in mixed crystals in dependence on the chemical composition (e.g., Fe^{3+} emission in the solid solutions of feldspar minerals) (Finch & Klein, 1999; Brooks et al., 2002; Krbetschek et al., 2002).

In relation to CL instrumentation, in general all types of equipment configured with an electron beam could potentially be used for CL analysis. A common technique is to realize CL measurements in scanning electron microscopes (SEMs) or microprobes (Edwards et al., 2003; MacRae et al., 2005). On the other hand, there exist combinations of electron guns with optical microscopes. Two general types of equipment can be distinguished—one using electron guns

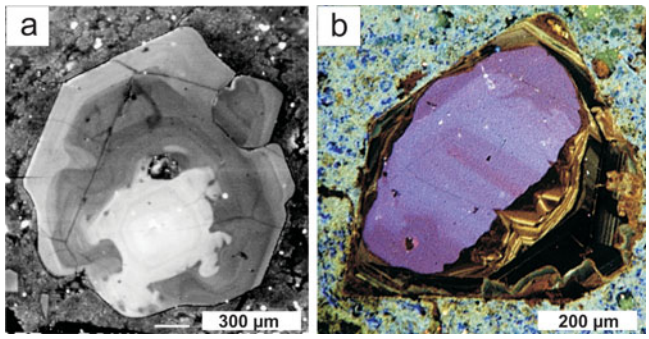

Figure 2. Comparison of panchromatic CL imaging in a SEM (**a**) with true color imaging in an optical CL microscope (**b**); the micrographs depict quartz crystals in volcanic rocks with complex internal textures.

with tungsten filaments (so called "hot-cathode" CL microscopes) and another one where the electron beam is generated by an ionized gas ("cold-cathode" CL microscopes).

A comparison of the different CL techniques reveals many similarities but also some significant differences, which have to be considered during the evaluation and discussion of analytical results (e.g., Marshall, 1988; Götze & Kempe, 2008). So, the generated electron beam in the SEM-CL is a scanning and focused beam, whereas CL microscopes use a stationary defocused beam. In addition, the use of mirror optics in SEM enables the analysis of the UV region, whereas the glass optics in CL microscopes absorbs the wavelength region below ca. 380 nm (see Götze & Kempe, 2008). Further differences between SEM-CL and CL microscopy exist, including panchromatic (gray levels) and true color imaging, respectively, and due to the different optical resolution (Fig. 2). Moreover, CL can be combined with backscattered electrons, secondary electrons, energy dispersive X-rays/wavelength dispersive X-rays in SEMs, whereas CL microscopes mainly allow a combination with polarized light imaging.

Table 1. Luminescence Emission Bands in Quartz and Related Defects.

Emission	Suggested Activator	References
175 nm (7.3 eV)	Intrinsic emission of pure SiO_2	Entzian & Ahlgrimm (1983)
290 nm (4.28 eV)	Oxygen vacancy	Jones & Embree (1976) Stevens-Kalceff (2009)
330–340 nm (3.75–3.6 eV)	Oxygen vacancy $[AlO_4/Li^+]$ center $[TiO_4/Li^+]$	Rink et al. (1993) Demars et al. (1996) Plötze & Wolf (1996)
380–390 nm (3.2–3.1 eV)	$[AlO_4/M^+]$ center; $M^+ = Li^+, Na^+, H^+$ $[H_3O_4]^0$ hole center	Alonso et al. (1983) Gorton et al. (1996) Yang & McKeever (1990)
450 nm (2.8 eV)	E_1' center with self-trapped exciton	Stevens-Kalceff & Phillips (1995) Skuja (1998)
500 nm (2.45 eV)	Extrinsic emission Interstitial impurity cations (Li^+, Na^+, H^+)	Itoh et al. (1988) Ramseyer & Mullis (1990) Perny et al. (1992) Götze et al. (2005)
580 nm (2.1 eV)	E′ center (oxygen vacancy)	Rink et al. (1993) Götze et al. (1999*a*)
620–650 nm (1.97–1.91 eV)	NBOHC with several precursors	Siegel & Marrone (1981) Stevens-Kalceff & Phillips (1995)
705 nm (1.7 eV)	Substitutional Fe^{3+}	Pott & McNicol (1971) Gorobets & Rogozine (2002)
1280 nm (0.97 eV)	Interstitial molecular O	Stevens-Kalceff (2009)

In general, the investigation of geological material requires a polished sample surface. Commonly, polished thin sections (48 × 28 mm, ca. 30 μm thick) are used that are transparent and enable the combination of CL studies with other analytical techniques such as polarizing microscopy, SEM, microprobe, or Raman spectroscopy. Polished thick sections (100–300 μm thick) are prepared for the combination of CL with, e.g., fluid inclusion studies. For SEM-CL and cold-cathode microscopes, the investigation of polished sections, polished sample surfaces, or even smooth surfaces of pressed powders (e.g., fine-grained clay minerals) is also possible (Götze & Kempe, 2009). The coating of samples with a thin conducting layer of C, Au, Ag, Cu, or Al is applied for high-energy electron beams to prevent any buildup of electrical charge during electron irradiation.

Cathodoluminescence Properties of Selected Minerals

In principle, minerals (insulators and semiconductors) of all mineral groups can show visible CL. Examples of CL active minerals are elements (e.g., diamond), sulfides (e.g., sphalerite), oxides (e.g., corundum, cassiterite, periclase), halides (e.g., fluorite, halite), sulfates (e.g., anhydrite, alunite, barite), phosphates (e.g., apatite), carbonates (e.g., calcite, aragonite, dolomite, magnesite, smithsonite), and silicates (e.g., feldspar, quartz, zircon, kaolinite, forsterite). In addition, several technical products such as synthetic minerals, ceramics, or glasses show interesting luminescence properties. No luminescence is produced by conductors, iron minerals, and most Fe-rich phases.

The interesting point for practical applications is the fact that there exists a close relationship between the specific conditions of formation, the real structure (specific defects), and the CL properties of minerals. Therefore, CL properties may provide important genetic information. This will be illustrated in the following examples by CL properties of selected minerals.

Quartz

Quartz and other minerals of the SiO_2 group are very interesting minerals for CL studies. In particular, quartz is one of the most abundant minerals in the Earth's crust (12.6 wt%) and also a widely used technological material. Comparison of the CL of natural quartz from different geological environments reveals drastic differences, which are mostly not visible in transmitted and polarized light (Ramseyer et al., 1988; Götze et al., 2001; Götze, 2009*a*).

These differences can be related to different defects in the real structure of quartz. The ideal structure of quartz is composed of a three-dimensional network of $[SiO_4]^{4-}$ tetrahedra, which may contain a couple of defects due to vacancies of oxygen or silicon, oxygen excess, or the incorporation of several trace elements (e.g., Al, Ti, Ge, Fe, P, H, Li, Na) (e.g., Götze, 2009*a*). More than 20 different types of those defects have been detected in quartz (e.g., Kostov & Bershov, 1987; Weil, 1984, 1993), which cause a range of luminescence emission bands in the UV, visible, and infra-

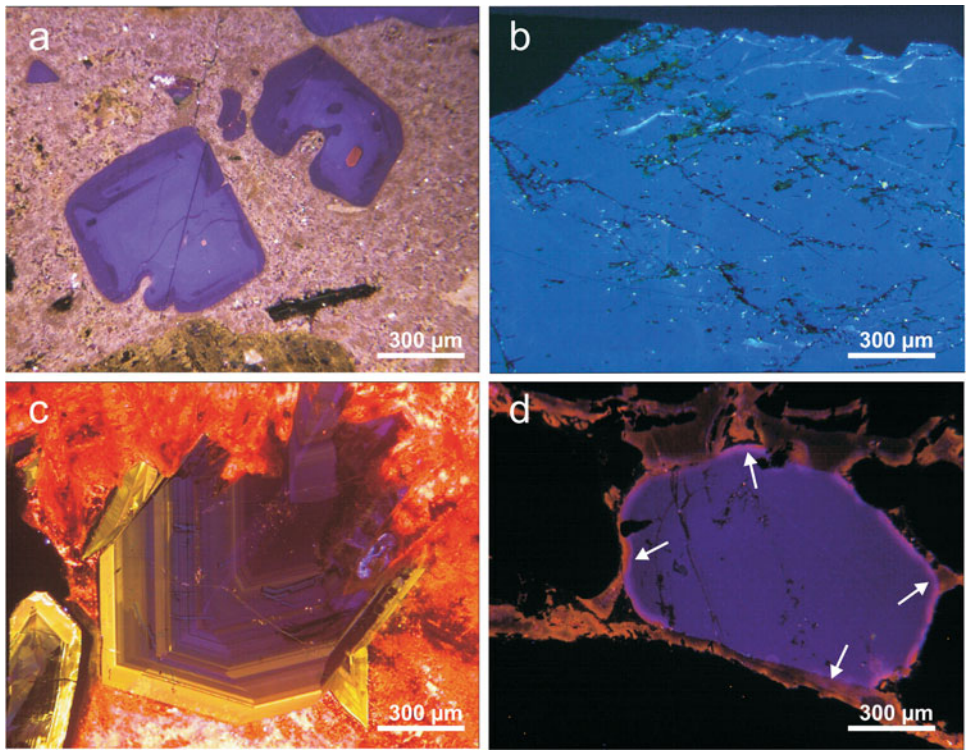

Figure 3. CL micrographs of quartz from different geological environments: (**a**) quartz in volcanic groundmass from Euba (Saxony, Germany) with growth zoning and resorption features; (**b**) homogeneous bluish-green pegmatite quartz from Evje-Iveland (Norway); (**c**) strongly zoned hydrothermal quartz crystal in calcite matrix from Khovd gol (Mongolia) showing both short-lived blue and yellow CL; (**d**) quartz grain from conglomerates in the Witwatersrand Au-U deposit (S-Africa), which exhibits radiation rims due to radioactive fluid flow (see arrows).

red (IR) region (see Table 1). The occurrence of specific luminescence emissions in quartz can often be related to specific conditions of formation (Ramseyer et al., 1988; Ramseyer & Mullis, 1990; Götze et al., 2001; Götze, 2009*a*).

The most common CL emission bands in natural quartz are the 450 and 650 nm band, respectively (Götze et al., 2001; Fig. 1b). These luminescence emissions are detectable in quartz crystals from magmatic and metamorphic rocks as well as authigenic quartz from sedimentary environments (Götze, 2012). In quartz of granites and granodiorites, the predominating 450 nm emission mostly causes visible CL colors in blue and violet, whereas quartz from volcanic rocks often shows zoning and violet-red CL due to a strong 650 nm emission (Fig. 3a). In quartz from pegmatite a transient emission around 500 nm is characteristic, which causes a greenish-blue CL color (Götze et al., 2005). This CL is unstable and disappears during electron irradiation (Fig. 3b). A short-lived blue CL (emission band at 390 nm) is the characteristic feature of natural and synthetic hydrothermal quartz (Ramseyer & Mullis, 1990; Perny et al., 1992; Götze et al., 2001). Often the decrease of the blue CL emission during electron bombardment is accompanied by an increase of the 650 nm emission resulting in a change of the initial blue CL color into reddish-brown (Fig. 3c). A typical yellow CL (emission band at ca. 580 nm) has been exclusively detected to date in natural hydrothermal quartz and cryptocrystalline chalcedony and agate and, therefore, is an important genetic indicator (Götze et al., 1999*c*; Götze, 2009*a*; Fig. 3c).

Alpha radiation due to the decay of radioactive elements (e.g., U, Th) can produce lattice defects [nonbridging oxygen hole center (NBOHC)], which are visible by a strong increase of the 650 nm emission. This behavior was detected both in radiation experiments (e.g., Komuro et al., 2002; Krickl et al., 2008) and natural samples (Owen, 1988; Meunier et al., 1990; Ramseyer et al., 1988; Götze et al., 2001; Botis et al., 2005). As a result, typical radiation halos develop in quartz due to contact with radioactive materials/fluids or around inclusions of minerals (e.g., zircon, monazite, uraninite) containing radioactive elements (Fig. 3d).

In several applications, specific CL colors of quartz have been used in geological studies. One of the most prominent is the use of quartz CL in the evaluation of the provenance of detrital material in sands and sandstones (e.g., Zinkernagel, 1978; Götze & Zimmerle, 2000; Richter et al., 2003; Götte & Richter, 2006). Assuming that the primary CL properties of quartz did not change during weathering, transport, and sedimentation, the spectrum of CL colors of detrital quartz grains reflects the source rocks of the sedimentary material. The different CL properties of primary detrital quartz grains and secondary diagenetic overgrowths also enable the detection of features associated with pressure solution and secondary quartz growth. These results provide important information concerning the dia-

Table 2. Luminescence Emission Bands in Feldspar Minerals and Related Defects.

Emission	Suggested Activator	References
280 nm (4.43 eV)	Tl^{+} Pb^{2+}	Gorobets et al. (1989) Tarashchan et al. (1973)
355 nm (3.5 eV)	Ce^{3+}	Laud et al. (1971)
420 nm (2.95 eV)	Eu^{2+} Cu^{2+}	Mariano & Ring (1975) Jaek et al. (1996)
450–480 nm (2.75–2.58 eV)	Al-O^{-}-Al center	Marfunin (1979) Walker (1985) Finch & Klein (1999)
	Al-O-Ti	Mariano et al. (1973) Lee et al. (2007) Parsons et al. (2008)
500–510 nm (2.48–2.43 eV)	O^{-}-Si . . . M^{+}	Marfunin & Bershov (1970)
550–570 nm (2.25–2.17 eV)	Mn^{2+}	Sippel & Spencer (1970) Götze et al. (2000)
690–740 nm (1.80–1.67 eV)	Fe^{3+}	Sippel & Spencer (1970) Finch & Klein (1999) Krbetschek et al. (2002)
860 nm	Pb^{+}	Erfurt (2003)
UV-Vis-IR	REE^{3+}	Mariano et al. (1973)
Several peaks		Götze et al. (1999*b*)

genetic history of sandstones, e.g., in the evaluation of potential oil reservoir sandstones (e.g., Houseknecht, 1991; Milliken & Laubach, 2000) or the characterization and differentiation of different kinds of recent and ancient building sandstones (e.g., Michalski et al., 2002; Götze & Siedel, 2004). Further applications are related to the characterization of hydrothermal mineralization processes (e.g., Graupner et al., 2000, 2001; Ioannou et al., 2003; Rusk et al., 2006, 2008) or the reconstruction of magmatic crystallization processes (e.g., Müller et al., 2000, 2002, 2003; Van den Kerkhof et al., 2004; Wark et al., 2007; Spear & Wark, 2009). There are also applications in the study of shock damage in quartz due to impact events, where features of microbrecciation and shifts of the luminescence emission bands under the influence of high pressure have been revealed by CL in terrestrial and extraterrestrial samples (e.g., Sippel, 1971; Ramseyer et al., 1992*a*; Boggs et al., 2001; Gucsik et al., 2003; Götze, 2009*b*).

Feldspar Minerals

Feldspar minerals belong to the most abundant and important group of rock-forming minerals. The minerals of this group cover the field of K, Na, and Ca alumo-silicates, the representâtives of which are K-feldspars (sanidine, orthoclase, microcline—$KAlSi_3O_8$) and the minerals of the plagioclase solid solution (albite $NaAlSi_3O_8$—anorthite $CaAl_2Si_2O_8$). The basic structural constituents of the MT_4O_8 alumosilicates are SiO_4 and AlO_4 tetrahedra (T-site) and interlattice positions of cations such as K, Na, or Ca (M-site), respectively. Accordingly, most feldspar minerals belong to the K-Na-Ca-series (orthoclase-albite-anorthite).

Several substitutions of elements in the T-site and M-site of natural feldspars exist, leading to the formation of other solid solutions such as the K-Ba series (hyalophane), $NaBSi_3O_8$ (reedmergnerite), or $NH_4AlSi_3O_8$ (buddingtonite). In addition, traces of other elements could be incorporated into the two structural sites (e.g., Fe, Ti, Ga, B on T-site and Ba, Sr, Rb, Mn, REE, Tl, Pb on M-site). Because of these defects and substitutions, a couple of luminescence emissions in the UV, visible, and IR region can be detected (Table 2). The most frequent defects in terrestrial and extraterrestrial feldspars responsible for CL are O^{-} defects, Mn^{2+} and Fe^{3+} (Marfunin & Bershov, 1970; Götze et al., 1999*a*, 2000; Kayama et al., 2010; Fig. 4).

The variety of luminescence emissions (colors and spectra) in feldspar minerals, which are dependent on pressure, temperature, and/or chemical environment (pTx conditions) of formation, causes a couple of applications. For instance, CL microscopy and spectroscopy can be applied to (1) differentiation of alkali feldspar and plagioclases (Fig. 5a), (2) detection of different feldspar generations, (3) visualiza-

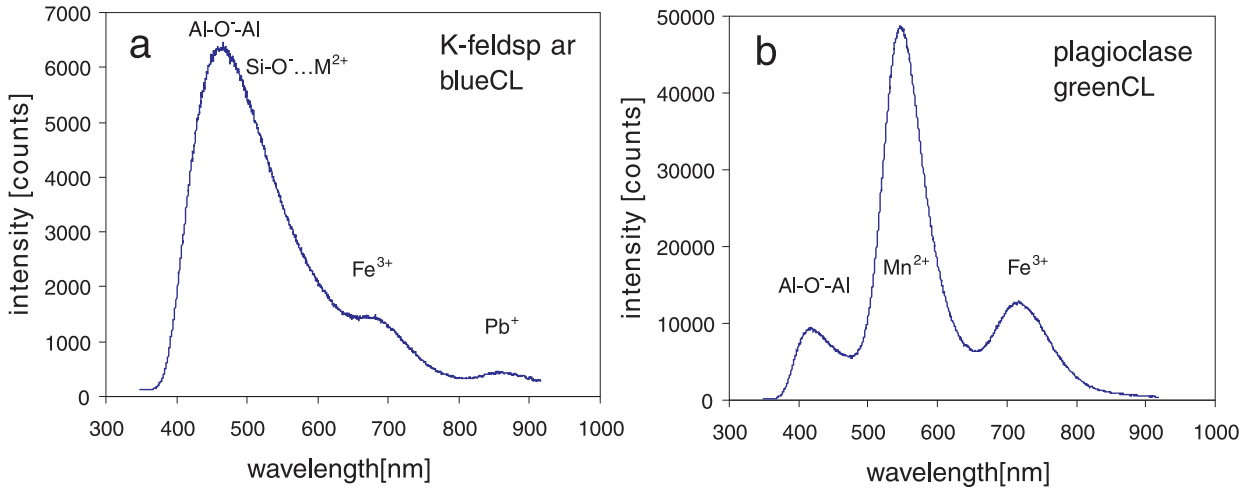

Figure 4. CL emission spectra of (**a**) K-feldspar and (**b**) plagioclase showing the most important emission bands due to O^{-} defects, Mn^{2+} and Fe^{3+}, respectively.

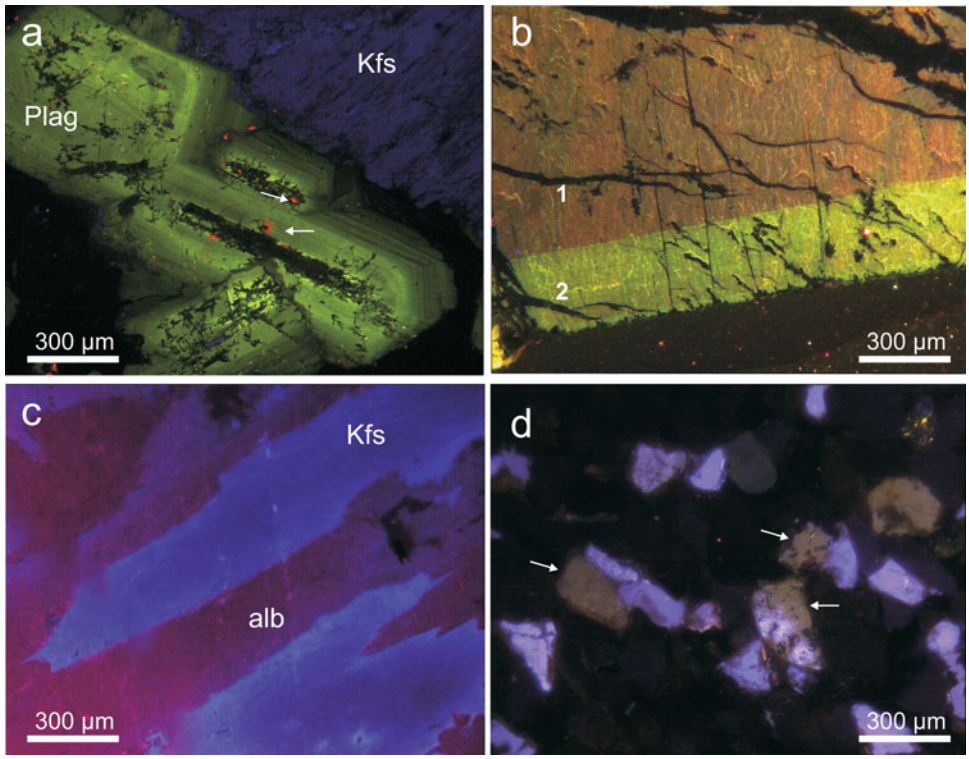

Figure 5. CL micrographs of feldspars from different geological environments: (**a**) strongly zoned plagioclase (Plag-green CL) and blue K-feldspar (Kfs) in a granite sample from Eibenstock (Saxony, Germany); the arrows point to orange spots of calcite; (**b**) anorthite from Monzoni (Italy) with red luminescent core (1 – Fe^{3+} activation) and green luminescent rim (2 – Mn^{2+} activation) indicating changes in the physicochemical conditions during crystal growth; (**c**) perthitic intergrowth of blue K-feldspar (Kfs) and reddish albite (alb); (**d**) sedimentary feldspar grains, which show features of weathering visible by a change of the primary blue CL into brownish (see arrows).

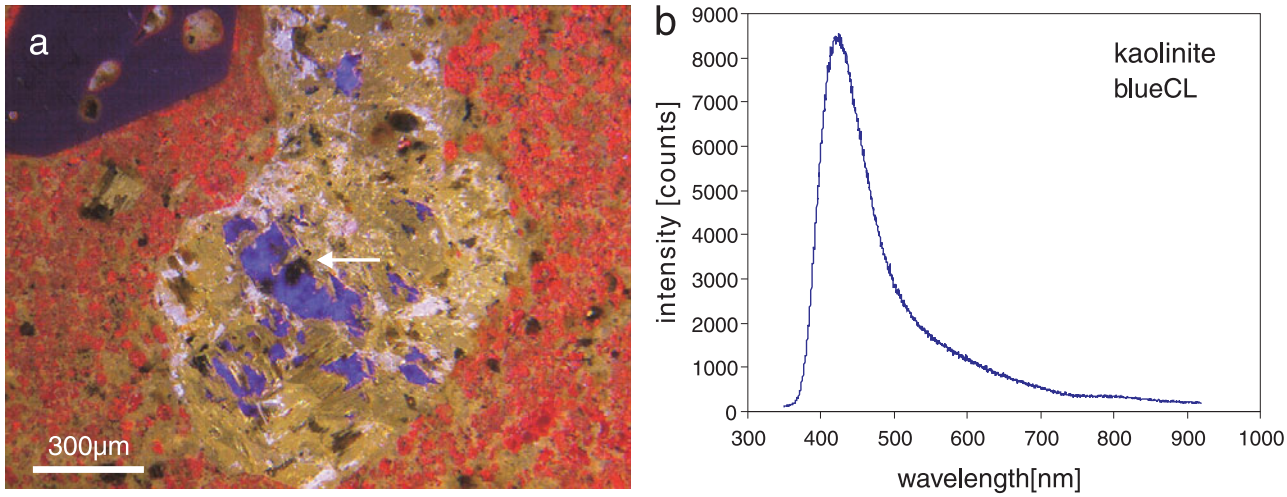

Figure 6. (**a**) CL micrograph showing starting kaolinization of a volcanic plagioclase; kaolinite is visible due to the deep blue CL (see arrow); (**b**) the related double emission peak in the CL spectrum around 400 nm is not fully visible because of the absorption in the UV due to the optical characteristics of the glass optics.

tion of internal structures and growth zoning (Figs. 5a–5c), (4) detection of alteration features such as weathering, albitization, and radiation damage (Fig. 5d), (5) detection of secondary authigenic overgrowths, or (6) rapid differentiation of quartz and feldspar (especially in fine-grained material). Primary growth structures in feldspar crystals can be related to varying abundances of lattice defects or activator ions. Such internal structures are often not visible in conventional microscopy and may represent trace-element variations in the ppm level (Fig. 5).

Secondary processes of weathering, alteration, or radiation damage are also detectable by CL. For example, in

alkali feldspar, weathering causes a change from initial blue CL (450 nm) to a brownish CL (590 nm emission) (Wendler et al., 2012). This is visible in altered grain parts and is probably caused by the formation of defects in the crystal structure (Fig. 5d). The secondary formation of Na-rich feldspar (albitization) during diagenesis is also detectable by CL (Ramseyer et al., 1992*b*; Richter et al., 2002). The chemical and structural changes result in a decrease of the CL intensity and the appearance of a new emission band at 620 nm (González-Acebrón et al., 2012). Last but not least, CL contributes to the study of radiation damage (Krickl et al., 2007; Kayama et al., 2011) and shock deformation (e.g., Gucsik et al., 2005; Kayama et al., 2006; Götze, 2009*b*) in feldspar minerals.

Sheet Silicates (Clay Minerals)

Sheet silicates represent another interesting group of silicate minerals. In particular certain clay minerals are important constituents of sediments, sedimentary rocks, and as raw materials (e.g., kaolinite—$Al_2[(OH)_4/Si_2O_5]$). A systematic evaluation of sheet silicates revealed that some of these minerals show a deep blue CL (kaolinite group, pyrophyllite—$Al_2[(OH)_2/Si_4O_{10}]$), whereas others do not luminesce (e.g., illite—$(K,H_2O)Al_2[(OH)_2/AlSi_3O_{10}]$) (Götze et al., 2002). An initial evaluation of clay minerals under the CL microscope can detect details of structure complementing other techniques.

Further studies by electron paramagnetic resonance indicated that the deep blue CL (double peak around 400 nm—see Fig. 6) is probably caused by electron defect centers on silicon-oxygen or Al-oxygen bonds, respectively (Götze et al., 2002). Investigations concerning the time-dependent behavior further revealed that one group shows decreasing CL intensity during electron irradiation (kaolinite), whereas the other group exhibits an intensity increase at the same time (dickite, pyrophyllite). This is visible by comparing irradiated and nonirradiated parts or by time-resolved measurements. The effect is probably caused by different types of electron defects ($Si\text{-}O^-$ or $Al\text{-}O^-\text{-}Al$) (Götze et al., 2002).

The knowledge of these CL properties enables the detection of weathering and alteration processes in minerals and rocks (Fig. 6) or to distinguish different pore cements in sedimentary rocks, which consist of fine-grained clay minerals with similar optical and crystallographic properties. Such information can be used to reconstruct weathering processes and conditions of diagenesis.

Carbonates

The carbonate mineral group consists of important rock-forming minerals, in particular in the sedimentary environment. The CL of carbonates is related to the presence and/or absence of activator ions (Mn^{2+}, $REE^{2+/3+}$), sensitizers (Pb^{2+}), and quenchers ($Fe^{2+/3+}$, Ni^{2+}, Co^{2+}), where Mn^{2+} is the most important activator ion (e.g., Marfunin, 1979; Marshall, 1988; Mason & Mariano, 1990; Machel & Burton, 1991; El Ali et al., 1993; Habermann et al., 1996, 1998, 2000; Götte & Richter, 2004). Furthermore, all carbonates may exhibit a luminescence emission band around 400 nm, which can probably be related to electron defects on the $[CO_3]$-group (Habermann et al., 1997).

Mn^{2+} is an activator ion with partially filled 3d orbitals in the outer shell, which can be influenced by the crystal field. Therefore, the wavelength of the Mn^{2+} emission band is characteristic of the crystal structure of the host mineral (influence of the crystal field). For example, tetrahedrally coordinated Mn^{2+} gives a green-yellow emission, whereas the emission from octahedrally coordinated Mn^{2+} is in the orange-red range (Marfunin, 1979). This effect can be observed for the Mn^{2+} activated luminescence in carbonates, which show shifting emission maxima (and with that visible luminescence colors) depending on the crystal type (Fig. 7a).

The Mn^{2+} activated CL in aragonite (rhombic $CaCO_3$) is green (emission band at ca. 580 nm), in calcite (trigonal $CaCO_3$) yellow (ca. 620 nm), and in magnesite (trigonal $MgCO_3$) red (ca. 655 nm). The visible orange-red CL of the double carbonate dolomite ($CaMg[CO_3]_2$) is composed of two overlapping bands with emission maxima at 575 nm (Mn^{2+} at Ca position) and 655 nm (Mn^{2+} at Mg position) resulting in asymmetric band profiles (Fig. 7b). The varying site occupancy can be related to different physicochemical conditions of formation and, therefore, provides important genetic information.

Cathodoluminescence in carbonates can be related to the common chemical zonation in diagenetic carbonate cements (compare Fig. 7b). A first highlight in CL petrography of zoned carbonate cements was published by Meyers (1974), who recognized the lateral and chronological correlation of cements from the Mississippian of New Mexico and developed the concept of cement stratigraphy. Several applications have shown the potential of CL studies in the reconstruction of carbonate diagenesis (e.g., Marshall, 1988; Machel & Burton, 1991; Meyers, 1991; Machel, 2000; Richter et al., 2003).

Apatite

Apatite $Ca_5[F/(PO_4)_3]$ is an important accessory mineral occurring in almost all rock types. In addition, apatite is an important constituent of biomaterials (bone and tooth) and laser materials. The incorporation of activator elements into the apatite lattice depends on the specific physicochemical conditions of crystallization. Therefore, the CL of apatite often reflects its origin and may differ in different rock types. For instance, pure apatite shows "intrinsic" blue CL (emission around 400 nm), which is caused by lattice defects (electron defects on oxygen of the phosphate group) (Habermann et al., 1997). Mn^{2+} activated CL is yellow, and REEs cause a violet or rose CL (compare Fig. 8). The incorporation of REE is enhanced by the coupled substitution $Ca^{2+} + P^{5+} \rightarrow REE^{3+} + Si^{4+}$, $2Ca^{2+} \rightarrow Na^+ + REE^{3+}$ or $3\,Ca^{2+} \rightarrow REE^{3+}$ + vacancy (e.g., Portnov & Gorobets, 1969; Rønsbo, 1989; Hughes et al., 1991*a*, 1991*b*; Rakovan & Reeder, 1996; Mitchell et al., 1997; Blanc et al., 2000). In contrast, the incorporation of Fe^{2+} or As^{5+} into the apatite structure can result in

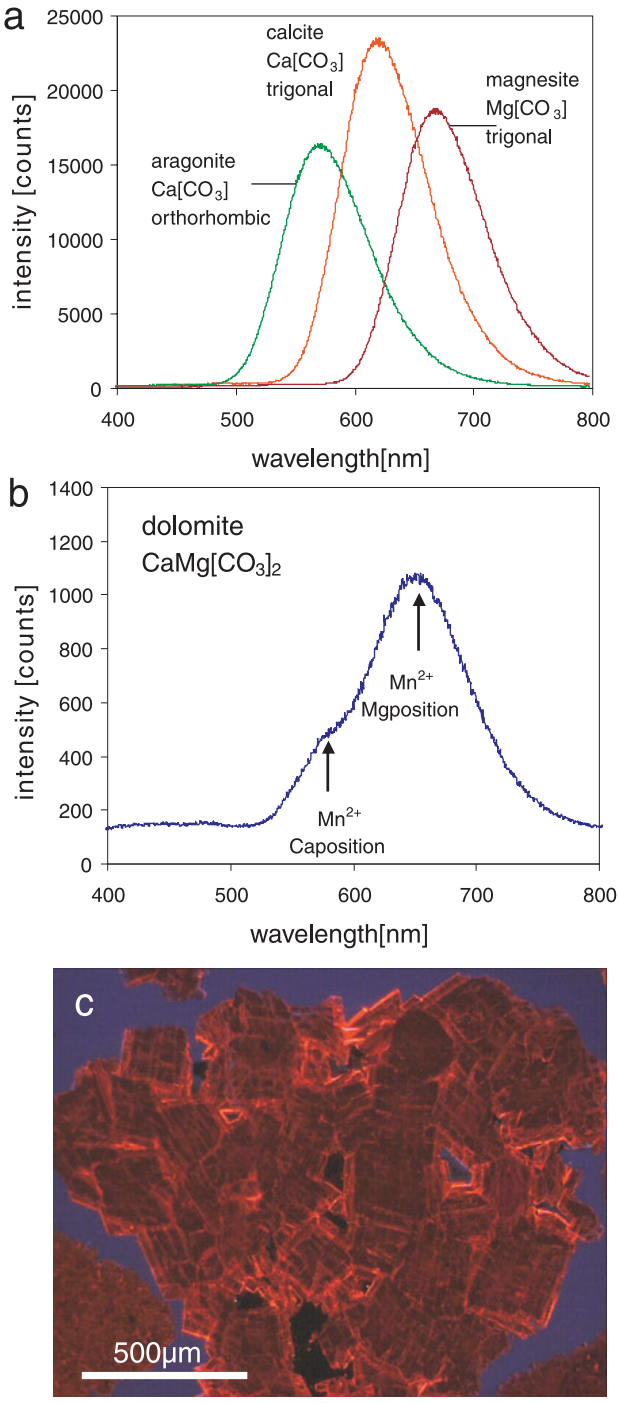

Figure 7. CL emission spectra of different carbonates (**a**) showing the shift of the Mn^{2+} activated CL in dependence on the crystal structure (local crystal field); (**b**) dolomite shows a double peak due to two different site occupancies of Mn^{2+} in Ca and Mg position, respectively; image **c** shows diagenetic dolomite cement with distinct zoning (width = 1.5 mm).

significant quenching of the luminescence intensity (Filippelli & Delaney, 1993; Perseil et al., 2000).

Based on this knowledge, the CL of apatite can be used to reconstruct geological processes or to get information about the physicochemical environment. Apatite from granites often luminesces yellow due to activation by Mn^{2+}, whereas apatites from alkaline rocks and carbonatites exhibit predominantly blue and violet CL colors due to REE activation (Kempe & Götze, 2002). The occurrence of yellow-violet zonation (Fig. 8) is an indicator for changing physicochemical conditions (alkaline—acidic) during crystallization (e.g., mixing of basic and acidic magma, see Slaby & Götze, 2004).

Zircon

Zircon ($Zr[SiO_4]$) is an accessory mineral that occurs widespread in crystalline and sedimentary rocks. The visible CL of zircon mainly shows bluish and yellowish colors (Fig. 9). The related CL spectra exhibit broad bands, which are caused by lattice defects and/or narrow emission lines due to the incorporation of trace elements such as REE. Dy^{3+} is the dominant activator element in all zircons, whereas other REEs such as Sm^{3+}, Tb^{3+}, Er^{3+}, Gd^{3+}, Nd^{3+} are of minor importance (Nasdala et al., 2003). Typical emission lines of the rare earth elements in synthetic zircon crystals are presented by Blanc et al. (2000).

An emission band centered at ca. 365 nm (visible as blue CL of many zircon grains) is probably caused by a delocalized electron on the $[SiO_4]$ groups similar to defects in many other silicates (e.g., Kempe et al., 2000). A typical broad emission band in the yellow region around 560 nm is of radiogenic origin in zircons that were exposed to radioactive irradiation (e.g., Remond et al., 2000; Kempe et al., 2000; Gaft et al., 2005; Nasdala et al., 2010).

The use of zircon CL in geosciences is widespread. Because of its chemical and mechanical resistance, zircon inherits a wealth of geological information and is widely used in heavy mineral analysis and isotope dating of various rock types (Nasdala et al., 2003 and references therein). Therefore, CL imaging of zircon crystals in isotope dating has developed to a routine technique and related publications are numerous. Cathodoluminescence enables visualization of internal structures, deformation and recrystallization structures, alteration features, and relictic cores of former existing zircon crystals (Fig. 9). All this information is indispensable for correct interpretation of isotope data.

Applications of CL in Geosciences

Cathodoluminescence has developed to a powerful analytical tool in geosciences and, therefore, applications are numerous. General topics include for example (1) the identification of minerals, mineral distribution, and quantification, (2) visualization of primary and secondary microstructures (growth zoning, deformation features, fluid flow, etc.), (3) crystal chemistry (trace element distribution, internal structures), (4) reconstruction of geological processes, and (5) characterization of technical products (Marshall, 1988; Barker & Kopp, 1991; Götze, 2000; Pagel et al., 2000; Gorobets & Rogozine, 2002; Gaft et al., 2005; Boggs & Krinsley, 2006; Gucsik, 2009).

Several applications have shown that a combination of CL with other analytical methods provides the best results.

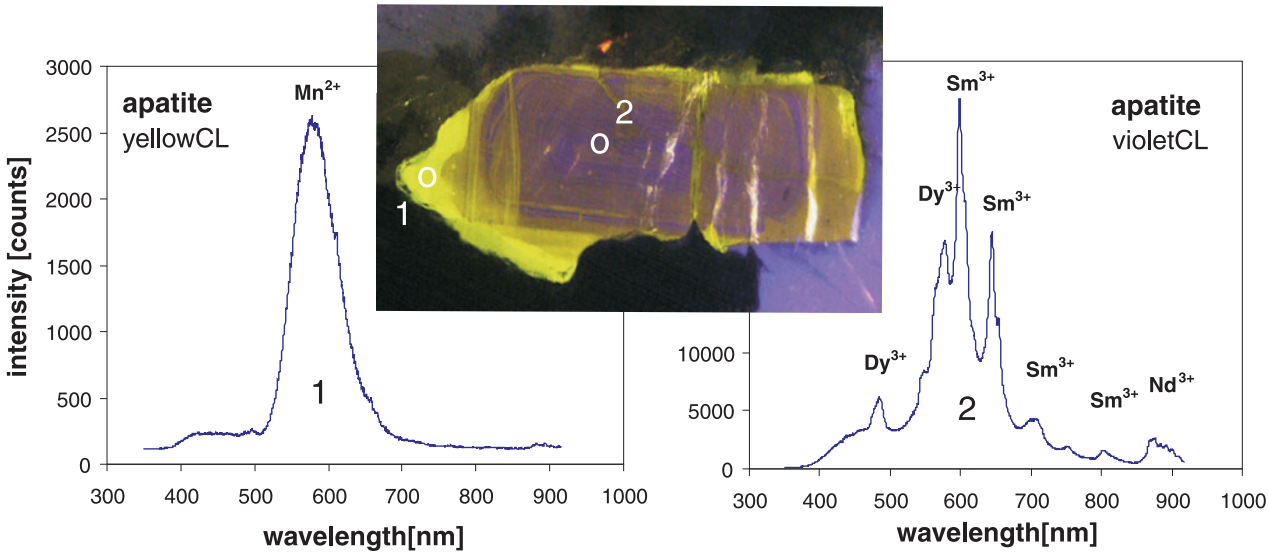

Figure 8. Apatite crystal in a granite from the Karkonosze pluton (Poland); the differently luminescent zones show activation by Mn^{2+} (yellow CL) and REE^{3+} (violet CL) indicating changes in physicochemical conditions during crystal growth.

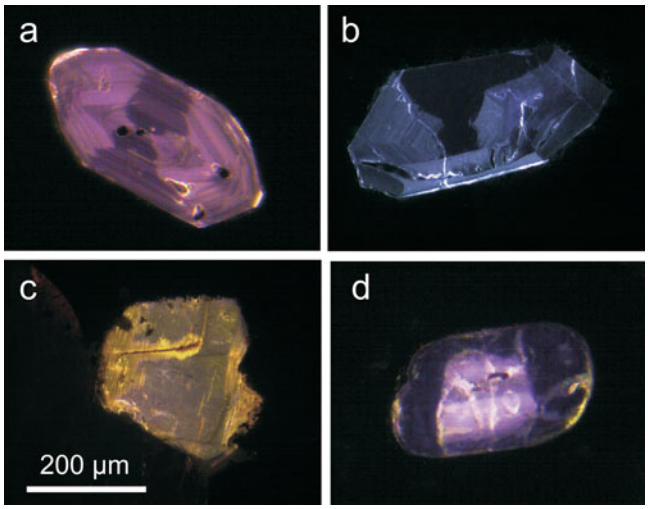

Figure 9. CL micrographs of zircon grains from different geological environments and with different internal textures: (**a**) zircon from granite with sector zoning and typical oscillatory zoning; (**b**) blue luminescent zircon crystal from the Mid-Atlantic ridge of probably hydrothermal origin; (**c**) zircon from a volcanic rock showing strong features of resorption and alteration; (**d**) rounded detrital zircon grain from a sediment with a relictic core, which is only discernable by CL.

Besides the combination of CL imaging with CL spectroscopy, other spatially resolved analytical methods offer potential for an integrated analytical approach. These are for example fluid inclusion studies, spatially resolved isotope analyses (e.g., SIMS dating, laser ablation isotope analysis), spatially resolved trace-element analyis (e.g., laser ablation inductively coupled plasma mass spectrometry, particle-induced X-ray emission, ion microprobe), micro-Raman spectroscopy and imaging, and/or Nomarski differential interference contrast microscopy. Often highly sensitive and spatially resolved analytical methods require CL studies to prove the homogeneity or heterogeneity of samples before the analytical work and to select useful analytical points/areas. Conversely, the additional analytical data can be used for the interpretation of the CL data.

Cathodoluminescence enables the rapid identification of minerals, even if they are present in small volumes and low concentration. Many accessory mineral phases or constituents with similar optical properties are overlooked in a conventional petrographic microscope (Fig. 10a).

Furthermore, the distinct CL color contrast of different mineral phases often allows the quantification of the amounts of certain minerals using modern image analysis systems (Evans et al., 1994; Götze & Magnus, 1997). However, identification and quantification by image analysis are not always possible. Low CL contrast or changes in CL colors due to chemical variations or alteration effects can limit the procedure.

Another important application of CL is the visualization of primary and secondary microstructures in minerals, which are not usually observable in conventional microscopy. These microstructures (e.g., oscillatory zoning, sector zoning, twinning/domains, chemical heterogeneities, microinclusions) help to reconstruct the growth conditions of minerals and to reveal secondary alteration processes such as deformation, fluid flow and related processes, recrystallization, or radiation damage. Oscillatory zoning is a common phenomenon observed in crystals grown from a melt or hydrothermal fluids (Figs. 9a, 9b). Sector zoning (Fig. 9a) is an indication for crystal growth under nonequilibrium conditions. Both are mostly not observable by conventional microscopy. Secondary features can also be detected by CL. A prominent application of CL is the visualization of secondary fluid trails in rocks and minerals (Fig. 10b). Another example is given by radiation damage features in minerals,

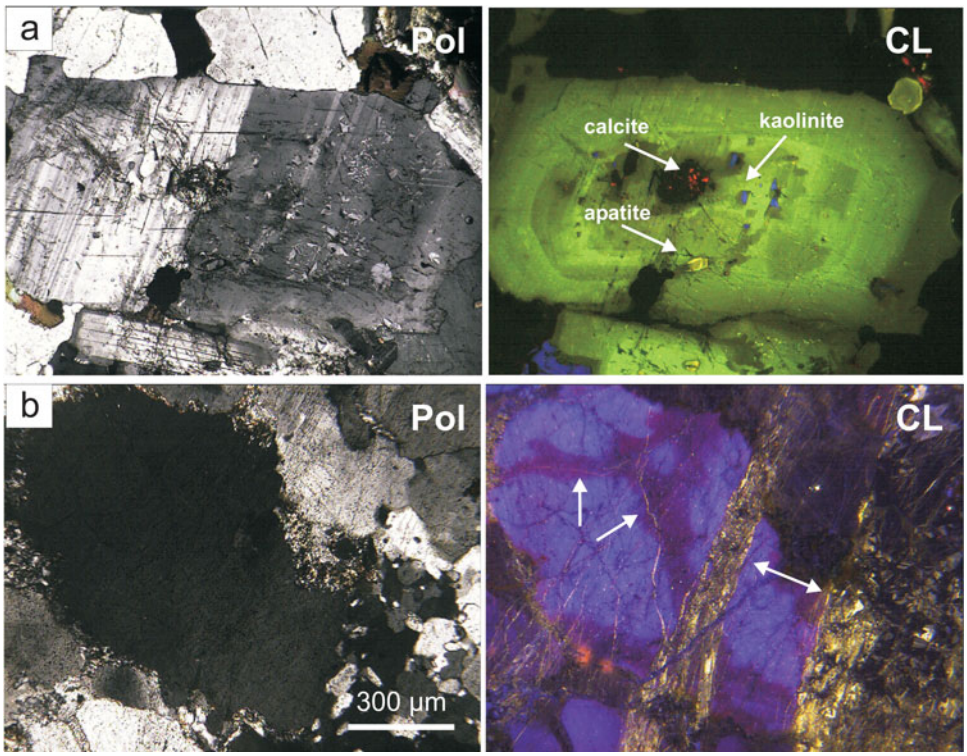

Figure 10. (**a**) Altered plagioclase crystal with minor inclusions of calcite, kaolinite, and apatite, which are visible in CL but not detectable in polarized light (Pol); (**b**) sandstone sample that clearly reveals features of secondary fluid flow in quartz grains (see arrows) not detectable in polarized light (Pol).

which can be detected by the formation of CL-active radiation halos due to alpha radiation (Fig. 3d).

The close relationship between trace element incorporation, related lattice defects, and CL properties of minerals opens up a broad field of applications in crystal chemistry. CL microscopy can reveal distinct zoning, which is caused by variations in the trace element composition or the growth conditions (Fig. 8).

In several studies a correlation of trace element (activator) concentrations and the related CL intensities was observed. Therefore, several authors have tried to quantify selected trace elements by combining spatially resolved CL spectroscopy with trace-element analysis (e.g., Habermann et al., 2000; Habermann, 2002; Götte & Richter, 2004; MacRae et al., 2009; Guguschev et al., 2010). However, for the quantification of trace elements, several factors have to be taken into account, which may influence the CL intensity. These are both analytical factors such as sample preparation and coating, analytical conditions, temperature, or the type of equipment and crystal-chemical factors such as luminescence activation, sensitizing and quenching, or time-dependent CL behavior. One of the dominant factors is the so-called "concentration quenching," a decrease of luminescence intensity caused by increasing activator concentration. This phenomenon can be explained by the preferred interaction of activator ions at high activator concentration, which prevents radiative transitions for luminescence activation. Another factor may be the ratio between potential activator and quencher ions, respectively, which influences the luminescence intensity more strongly than the activator concentration alone (Kempe & Götze, 2002).

The knowledge of specific CL properties of minerals and rocks enables the use of CL signatures for the reconstruction of geological processes. This is shown by an example of an albite sample, which seems to be homogeneous according to polarizing light microscopy (Fig. 11). However, CL reveals trails with different luminescence behavior (Mn^{2+} vs. REE^{3+} activated), which indicate a secondary alteration process. This conclusion was confirmed by locally resolved trace-element analysis of the different areas, which show different Mn contents and REE signatures, respectively (Götze et al., 1999*b*).

Last but not least, CL can be used for the investigation and characterization of technical products. Many materials such as ceramics, glasses, refractory materials, waste materials, building materials, or biomaterials show useful luminescence properties (Götze, 2000). Particular is the case of glasses or glass components, where CL studies are of important significance because the investigation of noncrystalline materials is difficult with most analytical methods. Moreover, with the help of CL, heterogeneities, or impurities in high-purity materials can be investigated, which are often not detectable by other analytical methods. The example in Figure 12 shows a high-purity Al_2O_3 ceramic, where impurities of Cr^{3+} are able to be detected by a combination of CL microscopy and spectroscopy. For example, these impurities are below the detection limit of microprobe analysis.

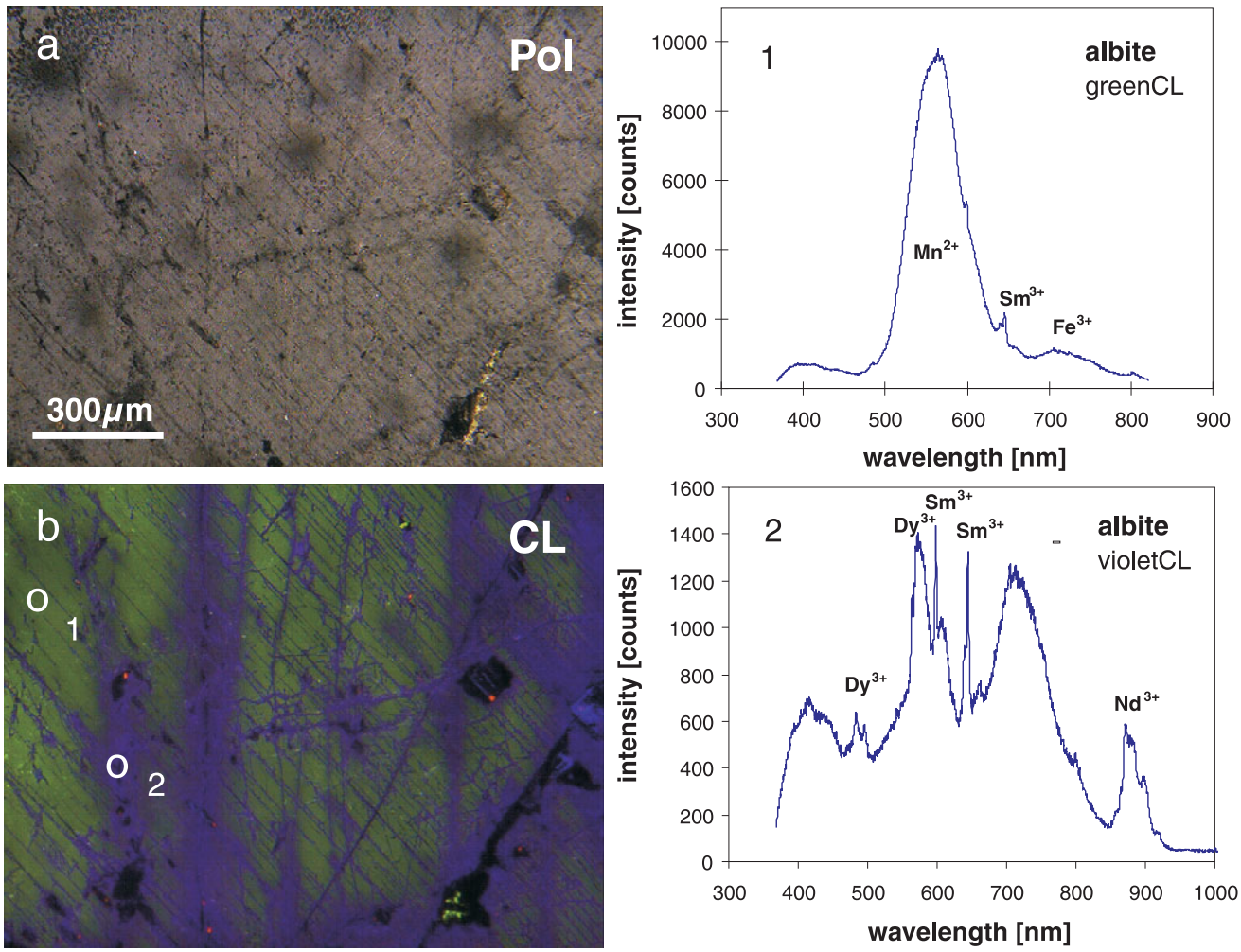

Figure 11. CL and polarized light micrograph pair of an albite sample from Spruce Pine (USA); the CL image clearly reveals alteration features, which are not discernable by conventional microscopy; CL spectra illustrate that the primary feldspar (green CL) is activated by Mn^{2+}, whereas the secondary trails are enriched in REE^{3+}.

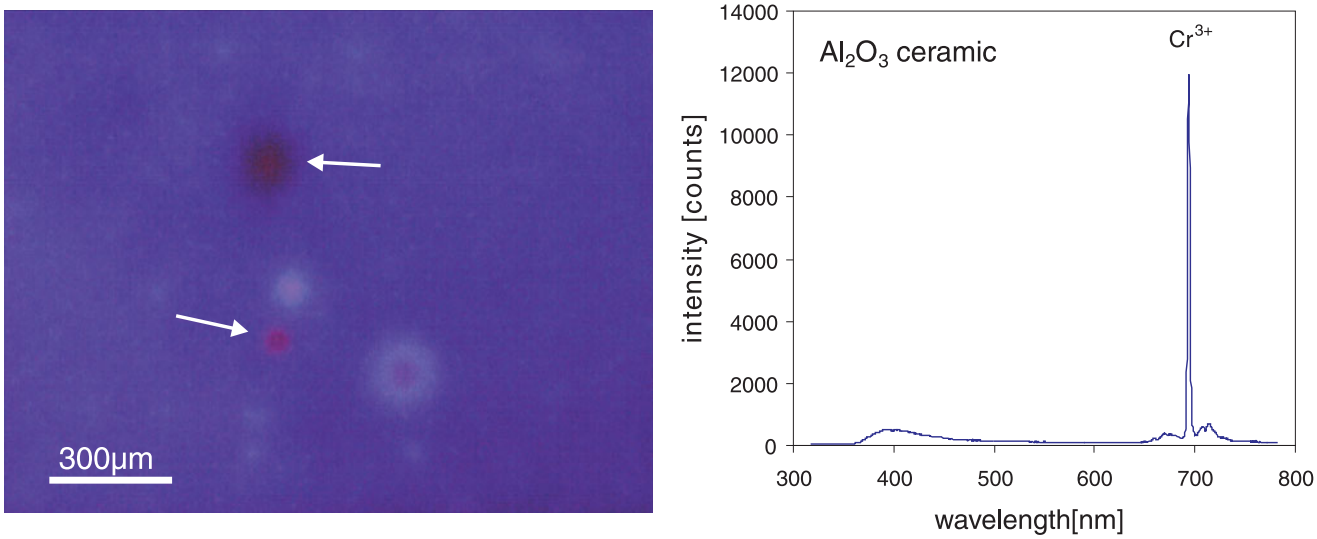

Figure 12. CL micrograph of high-purity Al_2O_3 ceramic with impurities visible as red spots; spectral CL analysis revealed the existence of chromium impurities below the detection limit of electron microprobe.

Conclusions

Cathodoluminescence is a common phenomenon in solids (minerals) that results from complex physical processes after excitation by an electron beam. Cathodoluminescence imaging and spectroscopy are luminescence techniques with widespread applications in geosciences. In previous years, a wealth of investigations have been performed on geomaterials to visualize growth textures and other internal textures that are not discernable with other analytical techniques, to use the information coming from CL studies for the reconstruction of processes of mineral formation and alteration, to provide information about the real structure of minerals and materials, and to prove the presence and type of lattice incorporation of several trace elements. Therefore, the close relation between specific conditions of mineral formation, real structure, and the CL properties may provide important genetic information concerning geological and technical processes.

The decoding and use of the luminescence signal require the knowledge of certain physical, crystallographic, and analytical interrelations. Although the principal processes in solids leading to luminescence are known, various specifics and interactions may significantly complicate the interpretation, especially in natural solids with mostly complex chemical composition. CL of minerals is predominantly a "defect luminescence,"; therefore, a combination of CL microscopy and spectroscopy can be used for the spatially resolved analysis of point defects. Best results will be obtained by combination of CL with other advanced analytical methods, the study of synthetic materials, and the simulation of "real" conditions of crystallization.

Acknowledgments

I gratefully acknowledge the comments of two anonymous reviewers and editorial handling by W. Jerome, which helped to improve the quality of the article.

References

Alonso, P.J., Halliburton, L.E., Kohnke, E.E. & Bossoli, R.B. (1983). X-ray induced luminescence in crystalline SiO_2. *J Appl Phys* **54**, 5369–5375.

Barker, C.E. & Kopp, O.C. (1991). *Luminescence Microscopy and Spectroscopy: Qualitative and Quantitative Applications*. Tulsa, OK: Society for Sedimentary Geology.

Blanc, P., Baumer, A., Cesbron, F., Ohnenstetter, D., Panczer, G. & Remond, G. (2000). Systematic cathodoluminescence spectral analysis of synthetic doped minerals: Anhydrite, apatite, calcite, fluorite, scheelite and zircon. In *Cathodoluminescence in Geosciences*, Pagel, M., Barbin, V., Blanc, P. & Ohnenstetter, D. (Eds.), pp. 127–160. Berlin, Heidelberg, New York: Springer.

Boggs, S., Jr. & Krinsley, H. (2006). *Application of Cathodoluminescence Imaging to the Study of Sedimentary Rocks*. Cambridge, UK: Cambridge University Press.

Boggs, S., Jr., Krinsley, D.H., Goles, G.G., Seyedolali, A. & Dypvik, H. (2001). Identification of shocked quartz by scanning cathodoluminescence imaging. *Mateor Planet Sci* **36**, 783–791.

Botis, S., Nokhrin, S.M., Pan, Y., Xu, Y. & Bonli, T. (2005). Natural radiation-induced damage in quartz. I. Correlations between cathodoluminescence colors and paramagnetic defects. *Can Mineral* **43**, 1565–1580.

Brooks, R.J., Finch, A.A., Hole, D.E., Townsend, P.D. & Wu, Z. (2002). The red to near-infrared luminescence in alkali feldspar. *Contrib Mineral Petrol* **143**, 484–494.

Burns, R.G. (1993). *Mineralogical Applications of Crystal Field Theory*, 2nd ed. Cambridge, UK: Cambridge University Press.

Demars, C., Pagel, M., Deloule, E. & Blanc, P. (1996). Cathodoluminescence of quartz from sandstones: Interpretation of the UV range by determination of trace element distributions and fluid-inclusion P-T-X properties in authigenic quartz. *Amer Mineral* **81**, 891–901.

Edwards, P.R., Martin, R.W., O'Donnell, K.P. & Watson, I.M. (2003). Simultaneous composition mapping and hyperspectral cathodoluminescence imaging of InGaN epilayers. *Phys Stat Sol* **7**, 2474–2477.

El Ali, A., Barbin, G., Cervelle, B., Ramseyer, K. & Bouroulec, J. (1993). Mn^{2+}-activated luminescence in dolomite, calcite and magnesite: Quantitative determination of manganese and site distribution by EPR and CL spectroscopy. *Chem Geol* **104**, 189–202.

Entzian, W. & Ahlgrimm, C. (1983). Comparing studies about the cathodoluminescence of SiO_2 (in German). *Wiss Zeit Uni Rostock, Naturwiss Reihe* **32**, 27–29.

Erfurt, G. (2003). Infrared luminescence of Pb^+ centres in potassium-rich feldspars. *Phys Stat Sol (a)* **200**, 429–438.

Evans, J., Hogg, A.J.C., Hopkins, M.S. & Howarth, R.J. (1994). Quantification of quartz cements using combined SEM, CL, and image analysis. *J Sed Res* **A64**, 334–338.

Filippelli, G.M. & Delaney, M.L. (1993). The effects of manganese(II) and iron(II) on the cathodoluminescence signal in synthetic apatite. *J Sed Petrol* **63**, 167–173.

Finch, A.A. & Klein, J. (1999). The causes and petrological significance of cathodoluminescence emissions from alkali feldspars. *Contrib Mineral Petrol* **135**, 234–243.

Gaft, M., Reisfeld, R. & Panczer, G. (2005). *Luminescence Spectroscopy of Minerals and Materials*. Berlin, Heidelberg, Germany: Springer.

González-Acebrón, L., Götze, J., Barca, D., Arribas, J., Mas, R. & Pérez-Garrido, C. (2012). Diagenetic albitization in the Tera Group, Cameros Basin (NE Spain) recorded by trace elements and spectral cathodoluminescence. *Chem Geol* **312–313**, 148–162.

Gorobets, B.S. & Rogozine, A.A. (2002). *Luminescent Spectra of Minerals*. Moscow, Russia: RPC VIMS.

Gorobets, B.S., Gaft, M.L. & Podolskiy, A.M. (1989). *Luminescence of Minerals and Ores*. Moscow: Ministry of Geology (in Russian).

Gorton, N.T., Walker, G. & Burley, S.D. (1996). Experimental analysis of the composite blue CL emission in quartz. *J Lumin* **72–74**, 669–671.

Götte, T. & Richter, D.K. (2004). Quantitative high-resolution cathodoluminescence spectroscopy of smithsonite. *Min Mag* **68**, 199–207.

Götte, T. & Richter, D.K. (2006). Cathodoluminescence characterization of quartz particles in mature arenites. *Sedimentology* **53**, 1347–1359.

Götze, J. (2000). *Cathodoluminescence Microscopy and Spectroscopy in Applied Mineralogy*. Freiberg, Germany: Freiberger Forschungsheft C 485.

Götze, J. (2009*a*). Chemistry, textures and physical properties of quartz—Geological interpretation and technical application. *Mineral Mag* **73**, 645–671.

Götze, J. (2009*b*). Cathodoluminescence microscopy and spectroscopy of lunar rocks and minerals. In *Cathodoluminescence and Its Application in the Planetary Sciences*, Gucsik, A. (Ed.), pp. 87–110. Berlin, Heidelberg, New York: Springer.

Götze, J. (2012). Mineralogy, geochemistry and cathodoluminescence of authigenic quartz from different sedimentary rocks. In *Quartz: Deposits, Mineralogy and Analytics*, Götze, J. & Möckel, R. (Eds.), pp. 287–306. Berlin, Heidelberg: Springer.

Götze, J., Habermann, D., Kempe, U., Neuser, R.D. & Richter, D.K. (1999*a*). Cathodoluminescence microscopy and spectroscopy of plagioclases from lunar soil (Luna20, Luna 24). *Amer Mineral* **84**, 1027–1032.

Götze, J., Habermann, D., Neuser, R.D. & Richter, D.K. (1999*b*). High-resolution spectrometric analysis of REE-activated cathodoluminescence (CL) in feldspar minerals. *Chem Geol* **153**, 81–91.

Götze, J. & Kempe, U. (2008). A comparison of optical microscope (OM) and scanning electron microscope (SEM) based cathodoluminescence (CL) imaging and spectroscopy applied to geosciences. *Mineral Mag* **72**, 909–924.

Götze, J. & Kempe, U. (2009). Physical principles of cathodoluminescence and its applications to geosciences. In *Cathodoluminescence and Its Application in the Planetary Sciences*, Gucsik, A. (Ed.), pp. 1–22. Berlin, Heidelberg, New York: Springer.

Götze, J., Krbetschek, M.R., Habermann, D. & Wolf, D. (2000). High-resolution cathodoluminescence studies of feldspar minerals. In *Cathodoluminescence in Geosciences*, Pagel, M., Barbin, V., Blanc, P. & Ohnenstetter, D. (Eds.), pp. 245–270. Berlin, Heidelberg, New York: Springer.

Götze, J. & Magnus, M. (1997). Quantitative determination of mineral abundance in geological samples using combined cathodoluminescence microscopy and image analysis. *Euro J Mineral* **9**, 1207–1215.

Götze, J., Plötze, M., Fuchs, H. & Habermann, D. (1999*c*). Defect structure and luminescence behaviour of agate—Results of electron paramagnetic resonance (EPR) and cathodoluminescence (CL) studies. *Miner Mag* **63**, 149–163.

Götze, J., Plötze, M., Götte, T., Neuser, R.D. & Richter, D.K. (2002). Cathodoluminescence (CL) and electron paramagnetic resonance (EPR) studies of clay minerals. *Mineral Petrol* **76**, 195–212.

Götze, J., Plötze, M. & Habermann, D. (2001). Origin, spectral characteristics and practical applications of the cathodoluminescence (CL) of quartz: A review. *Mineral Petrol* **71**, 225–250.

Götze, J., Plötze, M. & Trautmann, T. (2005). Structure and luminescence characteristics of quartz from pegmatites. *Amer Mineral* **90**, 13–21.

Götze, J. & Siedel, H. (2004). Microscopic scale characterization of ancient building sandstones from Saxony (Germany). *Mater Charact* **53**, 209–222.

Götze, J. & Zimmerle, W. (2000). Quartz and silica as guide to provenance in sediments and sedimentary rocks. *Contrib Sed Petrol* **21**, 1–91.

Graupner, T., Götze, J., Kempe, U. & Wolf, D. (2000). Cathodoluminescence imaging as a tool for characterization of quartz and trapped fluid inclusions in multistage deformed mesothermal Au-quartz vein deposits: A case study from the giant Muruntau Au-ore deposit (Uzbekistan). *Mineral Mag* **64**, 1007–1016.

Graupner, T., Kempe, U., Götze, J., Wolf, D., Irmer, G. & Kremenetsky, A.A. (2001). Au deposition and remobilization in the Muruntau "Central" quartz veins: Evidence from SEM, cathodoluminescence and fluid inclusion data. In *Mineral Deposits at the Beginning of the 21st Century*, Piestrzyński, A. et al. (Eds.), pp. 747–750. Lisse, The Netherlands: Swets & Zeitlinger Publishers.

Gucsik, A. (2009). *Cathodoluminescence and Its Application in the Planetary Sciences*. Berlin, Heidelberg, Germany: Springer.

Gucsik, A., Koeberl, Ch., Brandstätter, F., Libowitzky, E. & Reimold, W.U. (2003). Scanning electron microscopy, cathodoluminescence and Raman spectroscopy of experimentally shock-metamorphosed quartzite. *Meteor Planet Sci* **38**, 1187–1197.

Gucsik, A., Nishido, H., Ninagawa, K., Toyoda, S., Bidló, A., Brezsnyánsky, K. & Tsuchiyama, A. (2005). Cathodoluminescence spectral studies of the experimentally shock-deformed plagioclase: A possible explanation of CL peak shifts. *Lunar Planet Sci Conf XXXVI*, Abstract 1239.

Guguschev, C., Götze, J. & Göbbels, M. (2010). Cathodoluminescence microscopy and spectroscopy of synthetic ruby crystals grown by the optical floating zone technique. *Amer Mineral* **95**, 449–455.

Habermann, D. (2002). Quantitative cathodoluminescence (CL) spectroscopy of minerals: Possibilities and limitations. *Mineral Petrol* **76**, 247–259.

Habermann, D., Götze, J., Neuser, R. & Richter, D.K. (1997). The phenomenon of intrinsic cathodoluminescence: Case studies of quartz, calcite and apatite. *Zentralbl Geol Paläont Teil* **1, Heft 10–12**, 1275–1284.

Habermann, D., Neuser, R.D. & Richter, D.K. (1996). REE-activated cathodoluminescence of calcite and dolomite: High resolution spectrometric analysis of CL emission (HRS-CL). *Sed Geol* **101**, 1–7.

Habermann, D., Neuser, R. & Richter, D.K. (1998). Low limit of Mn^{2+}-activated cathodoluminescence of calcite: state of the art. *Sed Geol* **116**, 13–24.

Habermann, D., Neuser, R.D. & Richter, D.K. (2000). Quantitative high resolution spectral analysis of Mn^{2+} in sedimentary calcite. In *Cathodoluminescence in Geosciences*, Pagel, M., Barbin, V., Blanc, P. & Ohnenstetter, D. (Eds.), pp. 331–358. Berlin, Heidelberg, New York: Springer.

Houseknecht, D.W. (1991). Use of cathodoluminescence petrography for understanding compaction, quartz cementation, and porosity in sandstones. In *Luminescence microscopy: Quantitative and Qualitative Aspects*, Baker, C.E. & Kopp, O.C. (Eds.), pp. 59–66. Dallas, TX: SEPM.

Hughes, J.M., Cameron, M. & Crowley, K.D. (1991*a*). Ordering of divalent cations in the apatite structure: Crystal structure refinements of natural Mn- and Sr-bearing apatite. *Amer Mineral* **76**, 1857–1862.

Hughes, J.M., Cameron, M. & Mariano, A.M. (1991*b*). Rare-earth-element ordering and structural variations in natural rare-earth bearing apatite. *Amer Mineral* **76**, 1165–1173.

Ioannou, S.E., Götze, J., Weiershäuser, L., Zubowski, S.M. & Spooner, E.T.C. (2003). Cathodoluminescence characteristics of Archean VMS-related quartz: Noranda, Ben Nevis, and Matagami districts, Abitibi Subprovince, Canada. *G^3 Online Publication* **5**(2), DOI:10.1029/2003GC000613.

Itoh, C., Tanimura, K. & Itoh, N. (1988). Optical studies of self-trapped excitons in SiO_2. *J Phys C Solid State* **21**, 4693–4702.

Jaek, I., Hütt, G. & Vasiltchenko, E. (1996). Luminescence of the natural alkali feldspars artificially doped by Eu- and Cu-ions. *Third Europ Meeting Spectrosc Methods in Miner, Kiev, Progr & Abstr*, 23.

Jones, C.E. & Embree, D. (1976). Correlations of the 4.77–4.28 eV luminescence band in silicon dioxide with oxygen vacancy. *J Appl Phys* **47**, 5365–5371.

Kayama, M., Nakano, S. & Nishido, H. (2010). Characteristics of emission centers in alkali feldspar: A new approach by using cathodoluminescence spectral deconvolution. *Amer Mineral* **95**, 1783–1795.

Kayama, M., Nishido, H., Toyoda, S., Komuro, K. & Ninagawa, K. (2011). Radiation effects on cathodoluminescence of albite. *Amer Mineral* **96**, 1238–1247.

Kayama, M., Okumura, T., Nishido, H., Ninagawa, K. & Gucsik, A. (2006). Cathodoluminescence and Raman spectroscopy of shocked feldspar with PDFs. *Meteor Planet Sci* **41**(Suppl), 5180.

Kempe, U. & Götze, J. (2002). Cathodoluminescence (CL) behaviour and crystal chemistry of apatite from rare-metal deposits. *Mineral Mag* **66**, 135–156.

Kempe, U., Gruner, T., Nasdala, L. & Wolf, D. (2000). Relevance of cathodoluminescence for the interpretation of U-Pb zircon ages, with an example of an application to a study of zircons from the Saxonian Granulite Complex, Germany. In *Cathodoluminescence in Geosciences*, Pagel, M., Barbin, V., Blanc, P. & Ohnenstetter, D. (Eds.), pp. 425–456. Berlin, Heidelberg, New York: Springer.

Komuro, K., Horikawa, Y. & Toyoda, S. (2002). Development of radiation-damage halos in low-quartz: Cathodoluminescence measurement after He^{+} ion implantation. *Mineral Petrol* **76**, 261–266.

Kostov, R.I. & Bershov, L.V. (1987). Systematics of paramagnetic electron-hole centres in natural quartz (in Russ.). *Izvestiya Akademii nauk SSSR, Seria geologia* **7**, 80–87.

Krbetschek, M.R., Götze, J., Irmer, G., Rieser, U. & Trautmann, T. (2002). The red luminescence emission of feldspar and its wavelength dependence on K, Na, Ca–composition. *Mineral Petrol* **76**, 167–177.

Krickl, R., Götze, J. & Nasdala, L. (2007). New record of radiohaloes in feldspars. *Mitt Österr Miner Ges* **153**, Abstract.

Krickl, R., Nasdala, L., Götze, J., Grambole, D. & Wirth, R. (2008). Alteration of SiO_2 caused by natural and artificial alpha-irradiation. *Europ J Mineral* **20**, 517–522.

Laud, K.R., Gibbons, E.F., Tien, T.Y. & Stadler, H.L. (1971). Cathodoluminescence of Ce^{3+} and Eu^{2+}-activated alkaline earth feldspars. *J Electrochem Soc* **118**, 918–923.

Lee, M.R., Parsons, I., Edwards, P.R. & Martin, R.W. (2007). Identification of cathodoluminescence activators in zoned alkali feldspars by hyperspectral imaging and electron-probe microanalysis. *Amer Mineral* **92**, 243–253.

Machel, H.G. (2000). Application of cathodoluminescence to carbonate diagenesis. In *Cathodoluminescence in Geosciences*, Pagel, M., Barbin, V., Blanc, P. & Ohnenstetter, D. (Eds.), pp. 271–302. Berlin, Heidelberg, New York: Springer.

Machel, H.G. & Burton, E.A. (1991). Factors governing cathodoluminescence in calcite and dolomite, and their implications for studies of carbonate diagenesis. In *Luminescence Microscopy and Spectroscopy: Qualitative and Quantitative Applications*, Barker, C.E. & Kopp, O.C. (Eds.), pp. 37–58. Tulsa, OK: SEPM.

MacRae, C.M., Wilson, N.C. & Brugger, J. (2009). Quantitative cathodoluminescence mapping with application to a Kalgoorlie Scheelite. *Microsc Microanal* **15**(3), 222–230.

MacRae, C.M., Wilson, N.C., Johnson, S.A., Phillips, P.L. & Otsuki, M. (2005). Hyperspectral mapping—Combining cathodoluminescence and X-ray collection in an electron microprobe. *Microsc Res Techn* **67**(5), 271–277.

Marfunin, A.S. (1979). *Spectroscopy, Luminescence and Radiation Centres in Minerals*. Berlin, Germany: Springer.

Marfunin, A.S. & Bershov, L.V. (1970). Electron-hole centers in feldspars and their possible crystalchemical and petrological significance (in Russ.). *Dokl Akad Nauk* **193**, 412–414.

Mariano, A.N., Ito, J. & Ring, P.J. (1973). Cathodoluminescence of plagioclasi feldspars. *Geological Society of America, Abstract and Program* **5**, 726.

Mariano, A.N. & Ring, P.J. (1975). Europium-activated cathodoluminescence in minerals. *Geochim Cosm Acta* **39**, 649–660.

Marshall, D.J. (1988). *Cathodoluminescence of Geological Materials*. Boston, MA: Unwin-Hyman.

Mason, R.A. & Mariano, A.N. (1990). Cathodoluminescence activation in manganese bearing and rare-earth bearing synthetic calcites. *Chem Geol* **88**, 191–206.

Meunier, J.D., Sellier, E. & Pagel, M. (1990). Radiation-damage rims in quartz from uranium-bearing sandstones. *J Sed Petrol* **60**, 53–58.

Meyers, W.J. (1974). Carbonate cement stratigraphy of the Lake Valley Formation (Mississippian), Sacramento Mountains, New Mexico. *J Sed Petrol* **44**, 837–861.

Meyers, W.J. (1991). Calcite cement stratigraphy: An overview. In *Luminescence Microscopy and Spectroscopy: Qualitative and Quantitative Applications*, Barker, C.E. & Kopp, O.C. (Eds.), pp. 133–148. Tulsa, OK: SEPM.

Michalski, St., Götze, J., Siedel, H., Magnus, M. & Heimann, R.B. (2002). Investigations into provenance and properties of ancient building sandstones of the Zittau/Görlitz region (Upper Lusatia, Eastern Saxony, Germany). In *Natural Stone, Weathering Phenomena, Conservation Strategies and Case Studies*, Siegesmund, S., Vollbrecht, A. & Weiss, T. (Eds.), pp. 281–295. London: Geological Society Special Publications.

Milliken, K.L. & Laubach, S.E. (2000). Brittle deformation in sandstone diagenesis as revealed by scanned cathodoluminescence imaging with application to characterization of fractured reservoirs. In *Cathodoluminescence in Geosciences*, Pagel, M., Barbin, V., Blanc, P. & Ohnenstetter, D. (Eds.), pp. 225–242. Berlin, Heidelberg, New York, Tokyo: Springer.

Mitchell, R.H., Xiong, J., Mariano, A.N. & Fleet, M.E. (1997). Rare-earth-element-activated cathodoluminescence of apatite. *Can Mineral* **35**, 979–998.

Müller, A., Kronz, A. & Breiter, K. (2002). Trace elements and growth patterns in quartz: A fingerprint of the evolution of the subvolcanic Podlesi Granite System (Krušne Hory, Czech Republic). *Bull Czech Geol Surv* **77/2**, 135–145.

Müller, A., Rene, M., Behr, H.-J. & Kronz, A. (2003). Trace elements and cathodoluminescence of igneous quartz in topaz granites from the Hub Stock (Slavkovský Les Mts., Czech Rebublic). *Mineral Petrol* **79**, 167–191.

Müller, A., Seltmann, R. & Behr, H.J. (2000). Application of cathodoluminescence to magmatic quartz in tin granite—Case study from the Schellerhau Granite Complex, Eastern Ertgebirge, Germany. *Miner Deposita* **35**, 169–185.

Nasdala, L., Götze, J., Gaft, M., Hanchar, J. & Krbetschek, M. (2004). Luminescence techniques in earth sciences. *EMU Notes Mineral* **6**, 1–49.

Nasdala, L., Grambole, D., Götze, J., Kempe, U. & Váczi, T. (2010). Helium irradiation study on zircon. *Contr Mineral Petrol* **161**, 777–789.

Nasdala, L., Zhang, M., Kempe, U., Panczer, G., Gaft, M., Andrut, M. & Plötze, M. (2003). Spectroscopic methods applied to zircon. In *Zircon*, Hanchar, J.M. & Hoskin, P.W.O. (Eds.), pp. 427–467, Rev Mineral Geochem 41. Washington DC: Mineral Society of America.

Owen, M.R. (1988). Radiation-damage halos in quartz. *Geology* **16**, 529–532.

Pagel, M., Barbin, V., Blanc, P. & Ohnenstetter, D. (2000). *Cathodoluminescence in Geosciences*. Berlin, Heidelberg, New York: Springer.

Parsons, I., Steele, D.A., Lee, M.R. & Magee, C.W. (2008). Titanium as a cathodoluminescence activator in alkali feldspars. *Amer Mineral* **93**, 875–879.

Perny, B., Eberhardt, P., Ramseyer, K. & Mullis, J. (1992). Microdistribution of aluminium, lithium and sodium in quartz: Possible causes and correlation with short-lived cathodoluminescence. *Amer Mineral* **77**, 534–544.

Perseil, E.-A., Blanc, P. & Ohnenstetter, D. (2000). As-bearing fluorapatite in manganiferous deposits from St. Marcel-Praborna, Val D=Aosta, Italy. *Canad Mineral* **38**, 101–117.

Plötze, M. & Wolf, D. (1996). EPR- and TL-spectra of quartz: Irradiation dependence of (TiO_4^-/Li^+)-centers (in German). *Eur J Mineral, Bh* **8**, 217.

Portnov, A.M. & Gorobets, B.S. (1969). Luminescence of apatite from different rock types (in Russian). *Dokl Akademii Nauk SSSR* **184**, 110–115.

Pott, G.T. & McNicol, B.D. (1971). Spectroscopic study of the coordination and valence of Fe and Mn ions in and on the surface of aluminas and silicas. *Disc Faraday Soc* **52**, 121–131.

Rakovan, J. & Reeder, R. (1996). Intracrystalline rare earth element distributions in apatite: Surface structural influences on incorporation during growth. *Geochim Cosmochim Acta* **60**, 4435–4445.

Ramseyer, K., Aldahan, A.A., Collini, B. & Landstrom, O. (1992*a*). Petrological modifications in granitic rocks from the Siljan impact structure: Evidence from cathodoluminescence. *Tectonophysics* **216**, 195–204.

Ramseyer, K., Baumann, J., Matter, A. & Mullis, J. (1988). Cathodoluminescence colours of alpha-quartz. *Mineral Mag* **52**, 669–677.

Ramseyer, K., Boles, J.R. & Lichtner, P.C. (1992*b*). Mechanism of diagenetic albitization. *J Sed Petrol* **62**, 349–356.

Ramseyer, K. & Mullis, J. (1990). Factors influencing short-lived blue cathodoluminescence of alpha-quartz. *Amer Miner* **75**, 791–800.

Remond, G., Phillips, M.R. & Roques-Carmes, C. (2000). Importance of instrumental and experimental factors on the interpretation of cathodoluminescence data from wide band gap materials. In *Cathodoluminescence in Geosciences*, Pagel, M., Barbin, V., Blanc, P. & Ohnenstetter, D. (Eds.), pp. 59–126. Berlin, Heidelberg, New York: Springer.

Richter, D.K., Götte, T., Götze, J. & Neuser, R.D. (2003). Progress in application of cathodoluminescence (CL) in sedimentary geology. *Mineral Petrol* **79**, 127–166.

Richter, D.K., Götte, T. & Habermann, D. (2002). Cathodoluminescence of authigenic albite. *Sed Geol* **150**, 367–374.

Rink, W.J., Rendell, H., Marseglia, E.A., Luff, B.J. & Townsend, P.D. (1993). Thermoluminescence spectra of igneous quartz and hydrothermal vein quartz. *Phys Chem Miner* **20**, 353–361.

Rønsbo, J.G. (1989). Coupled substitution involving REEs and Na and Si in alkaline rocks from the Ilimaussaq intrusion, South Greenland and the petrological implications. *Amer Mineral* **74**, 896–901.

Rusk, B., Lowers, H.A. & Reed, M.H. (2008). Trace elements in hydrothermal quartz: Relationships to cathodoluminescent textures and insights into vein formation. *Geology* **36**, 547–550.

Rusk, B.G., Reed, M.H., Dilles, J.H. & Kent, A.J.R. (2006). Intensity of quartz cathodoluminescence and trace-element content in quartz from the porphyry copper deposit at Butte, Montana. *Amer Mineral* **91**, 1300–1312.

Siegel, G.H. & Marrone, M.J. (1981). Photoluminescence in as-drawn and irradiated silica optical fibers: An assessment of the role of nonbridging oxygen defect centres. *J Non-Cryst Sol* **45**, 235–247.

Sippel, R.F. (1965). Simple device for luminescence petrography. *Rev Sci Instrum* **36**, 556–558.

Sippel, R.F. (1971). Luminescence petrography of the Apollo 12 rocks and comperative features in terrestrial rocks and meteorites. *Proc Second Lunar Sci Conf* **1**, 247–263.

Sippel, R.F. & Spencer, A.B. (1970). Luminescence petrography and properties of lunar crystalline rocks and meteorites. *Proc Apollo 11 Lunar Sci Conf* **3**, 2413–2426.

Skuja, L. (1998). Optically active oxygen-deficiency-related centers in amorphous silicon dioxid. *J Non-Cryst Sol* **239**, 16–48.

Slaby, E. & Götze, J. (2004). Feldspar crystallization under magma mixing conditions evidenced by cathodoluminescence and geochemical modelling—A case study from Karkonosze pluton (SW Poland). *Mineral Mag* **68**, 541–557.

Smith, J.V. & Stenstrom, R.C. (1965). Electron-excited luminescence as a petrological tool. *J Geol* **73**, 627–635.

Spear, F.S. & Wark, D.A. (2009). Cathodoluminescence imaging and titanium thermometry in metamorphic quartz. *J Metam Geol* **27**, 187–205.

Stevens-Kalceff, M.A. (2009). Cathodoluminescence microcharacterization of point defects in α-quartz. *Miner Mag* **73**, 585–606.

Stevens-Kalceff, M.A. & Phillips, M.R. (1995). Cathodoluminescence microcharacterization of the defect structure of quartz. *Phys Rev B* **52**, 3122–3134.

Tarashchan, A.N., Serebrennikov, A.I. & Platonov, A.N. (1973). Features of lead ions luminescence in amazonite. *Constitutions and Properties of Minerals* **7**, 106–111 (in Russian).

Van den Kerkhof, A.M., Kronz, A., Simon, K. & Scherer, T. (2004). Fluid-controlled quartz recovery in granulite as revealed by cathodoluminescnece and trace element analysis (Bamble sector, Norway). *Contr Mineral Petrol* **146**, 637–652.

Walker, G. (1985). Mineralogical applications of luminescence techniques. In *Chemical Bonding and Spectroscopy in Mineral Chemistry*, Berry, F.J. & Vaughan, D.J. (Eds.), pp. 103–140. Birmingham, UK: University of Birmingham.

Wark, D.A., Hildreth, W., Spear, F.S., Cherniak, D.J. & Watson, E.B. (2007). Pre-eruption recharge of the Bishop magma system. *Geology* **35**, 235–238.

Weil, J.A. (1984). A review of electron spin spectroscopy and its application to the study of paramagnetic defects in crystalline quartz. *Phys Chem Miner* **10**, 149–165.

Weil, J.A. (1993). A review of the EPR spectroscopy of the point defects in α-quartz: The decade 1982–1992. In *Physics and Chemistry of SiO_2 and the Si-SiO Interface 2*, Helms, C.R. & Deal, B.E. (Eds.), pp. 131–144. New York: Plenum Press.

Wendler, J., Köster, J., Götze, J., Kasch, N., Zisser, N., Kley, J., Pudlo, D., Nover, G. & Gaupp, R. (2012). Carbonate diagenesis and feldspar alteration in fault-related bleaching zones (Buntsandstein, Central Germany)—Possible link to CO_2-influenced fluid-mineral reaction. *Int J Earth Sci* **101**, 159–176.

Yang, X.H. & McKeever, S.W.S. (1990). Point defects and predose effect in quartz. *Radiat Protect Dosim* **33**, 27–30.

Zinkernagel, U. (1978). Cathodoluminescence of quartz and its application to sandstone petrology. *Contr Sed* **8**, 1–69.